SOIL DRYING AND HEAT–MOISTURE DYNAMICS UNDER SIMULATED SOLAR RADIATION USING INFRARED ENERGY

Ágnes BÁLINT[1], Norbert NAGY[2], Xuechu WANG[2], Csaba MÉSZÁROS[2]
DOI: 10.12700/STAR.2026.142
[1]Obuda University, Institute of Environmental Engineering and Natural Sciences, Budapest, Hungary,
[2] Hungarian University of Agriculture and Life Sciences, Gödöllő, Hungary

Abstract:
The soil's water and energy balance play a fundamental role in regulating the hydrological cycle and near-surface climatic conditions. Previous studies have demonstrated that coupled heat and moisture transport processes strongly affect soil evaporation and temperature dynamics. Building on this foundation, our study investigated the drying behaviour of soil columns exposed to infrared radiation simulating solar energy, with particular focus on heat and mass transfer at the soil-air interface.
Laboratory experiments were performed on soil samples of different initial moisture conditions, including natural, water-saturated, and frozen states. Each experiment involved 12 hours of infrared exposure followed by 12 hours without irradiation, forming a 48-hour day–night cycle. Temperature and moisture content were measured at three depths, while surface temperature patterns and airflow dynamics were monitored with an infrared camera.
Results showed pronounced temperature fluctuations and moisture loss in the upper soil layers. Infrared imagery clearly revealed convective airflows forming above the soil columns during heating.
The experimental setup proved effective for analysing coupled heat and moisture transport. These findings enhance understanding of soil evaporation mechanisms and contribute to the development of sustainable soil–water management strategies.

Keywords: Convective boundary layer, Environmental sustainability, Heat and mass transport, Infrared-induced soil drying, Soil–atmosphere interactions

1. INTRODUCTION

The exchange of heat and mass between the soil surface and the overlying atmosphere represents one of the most dynamic components of the land–atmosphere system. The soil–atmosphere interface controls the partitioning of net radiation among sensible heat flux, latent heat flux, and ground heat flux, thereby regulating near-surface temperature gradients and boundary-layer development [1-3]. Variations in soil thermal properties, including volumetric heat capacity and thermal conductivity, strongly influence the temporal evolution of soil temperature profiles and the diurnal propagation of thermal waves [4-6]. Recent studies have emphasised that soil temperature and soil heat flux dynamics play an increasingly important role in climate feedback processes. Global analyses reveal systematic patterns in which soil temperature may exceed air temperature under certain radiative and moisture conditions, thereby altering surface energy partitioning and near-surface atmospheric stability [7]. Similarly, multi-scale investigations demonstrate that soil thermal dynamics significantly influence the diurnal development of the atmospheric boundary layer [8-9]. Advances in observational and modelling approaches have further improved the representation of soil heat flux in land surface schemes, highlighting the importance of accurate subsurface measurements [10-12]. Convective processes emerging above heated surfaces are governed by temperature gradients and buoyancy forces, representing classical non-equilibrium thermodynamic phenomena [13]. When the Rayleigh number exceeds a critical threshold, organised convective structures may develop, ranging from small-scale cellular convection to turbulent plumes [14]. In natural environments, surface heating during the day induces unstable stratification in the surface layer, promoting convective transport and vertical mixing [15-16]. Contemporary research demonstrates that land surface thermal heterogeneity substantially modifies convective available potential energy (CAPE) and may influence convective initiation and precipitation patterns [17-18]. Soil moisture gradients have also been shown to enhance mesoscale convection by modulating sensible and latent heat fluxes [19-20]. Soil moisture plays a central role in regulating the coupling strength between the land surface and the atmosphere. It affects evaporative fluxes, modifies the partitioning of available energy, and influences boundary layer growth [21-22]. Modern climate feedback analyses confirm that soil moisture–precipitation interactions constitute a key uncertainty in regional climate projections [23]. Remote sensing and in situ observational studies further demonstrate that variations in soil texture and moisture distribution significantly alter surface energy exchange processes [24-26]. The diurnal radiative cycle introduces periodic thermal forcing at the soil surface, generating time-dependent temperature gradients that propagate downward into the soil and upward into the atmospheric surface layer. The resulting cyclic heating and cooling strongly influence the stability regime of the near-surface air and modulate convective intensity [27-28]. Numerical investigations indicate that an accurate representation of diurnal soil temperature evolution is crucial for modelling land–atmosphere coupling and boundary-layer dynamics [29-30]. Despite substantial progress in large-scale observational and modelling studies, controlled experimental investigations of soil column systems under well-defined radiative forcing remain limited. Laboratory-scale experiments allow the isolation of key physical mechanisms governing coupled heat and moisture transport, as well as the emergence of convective air motions above the surface. Such controlled systems provide high-resolution vertical profiles of temperature and moisture, enabling quantitative assessment of energy partitioning and transient responses to periodic forcing.

In this study, we investigate bare soil columns subjected to controlled infrared irradiation in a 12 h light / 12 h dark cycle designed to simulate the diurnal solar forcing. Temperature was continuously measured in the air above the soil surface, at the surface itself, and within the soil at approximately 10 cm vertical intervals. Simultaneously, volumetric soil moisture content was monitored at corresponding depths using sensor-based measurements. This experimental setup enables the coupled analysis of subsurface thermal propagation, moisture redistribution, and near-surface atmospheric response under periodic radiative forcing. By integrating detailed vertical measurements with contemporary land–atmosphere interaction theory, our objective was to characterise the transient evolution of temperature gradients, identifying conditions conducive to convective instability, and quantify the relationship between soil drying dynamics and variability in near-surface air temperature. The results provide insight into microscale energy exchange processes and may contribute to improved parameterisation of soil heat and moisture fluxes in land-surface and boundary-layer models.

2. MATERIALS AND METHODS

2.1. Use of infrared radiation

Infrared radiation is a wavelength range of electromagnetic radiation between 0.78 µm and 1000 µm. Most of the energy from the Sun that reaches the Earth's surface is in the infrared. Infrared radiation can be divided into several ranges. These are the near-infrared (NIR, IR-A, 0.75-1.4 µm), the short-wavelength infrared (SWIR, IR-B, 1.4-3 µm), the mid-wavelength infrared (MWIR, IR-C, 3-8 µm), the far-infrared (FIR, 15-1000 µm) and the long-wavelength infrared (LWIR, IR-C, 8-15 µm). The total radiation reaching the Earth's surface consists of infrared and visible light. Optimally, 45% of the global surface radiation energy, about 450-500 W/m^2, falls in the infrared range, compared to the total of 1120 W/m^2. The wavelength of visible light falls in the range of about 380 nm to 760 nm, which represents the remaining part of the surface radiation, about 50-55%. The infrared wavelength range above 3 µm is largely absorbed by the atmosphere. Infrared energy passes through the air with almost no loss (IR-

A, IR-B). As a result, infrared rays heat up more than 80% of the body itself and less than 20% of the surrounding air. Since the effects of thermal radiation were investigated, the Sun's heating radiation was modelled using an infrared-emitting lamp (Philips Infrared R95E). The lamp's spectral energy has a maximum near 1 µm. As shown in Figure 1, the lamp emits predominantly in the near- and short-wavelength regions, whereas emission above 3 µm is negligible. The 24-hour orbit of the Sun is neglected; the lamp is emitted from a fixed point at a height of 400 mm, perpendicular to the surface of the cylindrical ground columns, from which the deeper layers of the ground are gradually heated.

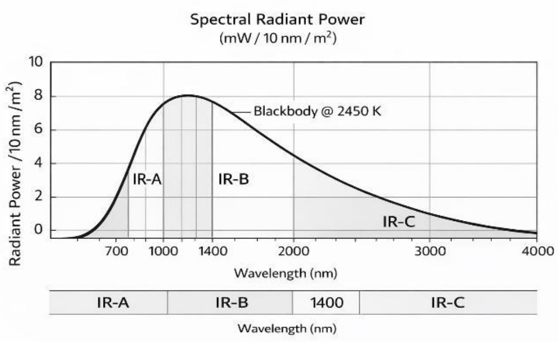

Figure 1: Spectral energy distribution of a 2450 K tungsten infrared lamp calculated from Planck's radiation law. The infrared regions (IR-A, IR-B, IR-C) are indicated according to ISO wavelength classification.

2.2. The soil columns and their saturation with water

A total of 2 quasi-undisturbed soil samples of different textures and physical properties were used in the experiments. The soil sample 1 is a sandy soil from a riverbed, and the soil sample 2 is a meadow soil. During the preparation of the soil samples, a slight degradation of the soil structure was unavoidable; therefore, the samples can be considered quasi-undisturbed. When the plastic pipe, 160 mm in diameter and 200 mm long, was buried in the soil, the structure may have been slightly damaged. At depths of 60, 120, and 180 mm below the soil surface, we made circular openings in each of the three soil columns, with a circular cross-section on each side corresponding to the width of the temperature sensors and soil tensiometers. We removed plastic elements 50 mm wide and 180 mm long from the surfaces of the two plastic columns and insulated them with plastic foil. The vertical temperature changes were subsequently monitored on this free ground surface using the infrared camera. A total of three measurements, each lasting 48 hours, were made with the aforementioned soil columns. The soils were prepared in different ways before the experiment. We present some results from two of our experiments:

First experiment: We started the experiment with soil column 1 in its original moisture state after sampling.

Second experiment: the soil column 2 was pre-saturated with water and then subjected to a 12-hour freeze immediately prior to measurement.

The saturation of the soil columns [32] with water was achieved using the principle of moving vessels to minimise changes in soil structure. We designed a closed water-saturation system in which water flows out of the vessel at a higher level than the soil column through a plastic tube attached to the vessel and to the bottom of the soil column, thereby saturating the porous soil structure. By this method, we also tried to change the soil structure as little as possible. The saturation time is about 24 hours, depending on the soil sample.

2.3. Sensors used for the measurement

Sensors were used to measure the temperature and moisture variations at three depths from the soil column surface, at the soil column surface and at a point laterally above the soil column surface during the 48-hour experiments. Temperature measurements were taken with an infrared camera at 120-second intervals in the airspace above the soil surface (160 x 160 mm^2) and on the soil surface (180 mm). The sensors were located and named as follows: One temperature sensor (TYPE K ZA-9020-FS NiCr-Ni BE NiCr °C) and one tensiometer (Ahlborn Insertion Tensiometer) were placed at a depth of 60 mm, 120 mm and 180 mm from the soil surface (Figure 2). The soil surface temperature was measured with a simple temperature plate sensor. A combined temperature-relative humidity sensor was set up on a stand on the side above the soil surface, at a point not directly exposed to the infrared light, to provide information on the air changes in the experimental enclosure. The temperature and relative humidity values were converted to vapour pressure (e) using the Magnus-Tettens [31] formula and then to absolute humidity values (a, [g/m^3]) using a simple relationship (0.217*e/T). The tensiometer used in the experiments was a plastic tube filled with water and a porous ceramic tip connected to a digital sensor, which is permeable to water but impermeable to air. The ceramic tip of the tensiometer, pre-boiled in distilled water and filled with bubble-free water, was measured at three different depths in the soil. The suction force of the soil solid phase draws water from the soil into the tip. Since no air can enter the closed interior of the tensiometer from outside, the leakage of water creates a vacuum in the interior, the extent of which is recorded by the manometer. The tensiometer actually measures the pressure, which is the 'suction' of the soil moisture, and the sensor tensiometer we use has a range of 0-900 hPa. The vacuum reading on the manometer can be converted to water column length (cm), and the moisture content corresponding to the measured tensiometer reading can be read directly from the soil's pF curve. As the soil dries, tensiometry increases in direct proportion to the continued drying [32].

2.4. Above-ground measurement surface system and infrared camera

In a previous experiment, measuring heat fluxes in the space above the soil surface was problematic because the infrared camera could only measure temperature on solid surfaces and not in air. A measurement surface system was designed to solve this problem (Figure 3). The surface system was formed from strips of paper, and the correct support and spacing were set using Styrofoam elements. The surface system consisted of 16 vertical paper surface slices, the first and third 5-5, the second 6 and 1 more horizontal at the bottom of the first layer. The paper surface slices did not overlap, allowing spatial measurement of temperature above the ground surface. The parallel layers were placed 40 mm apart. As can be seen in Figure 2, the surface system was located within a 160*160 mm^2 area, 180 mm above the ground surface. The elements of the measurement surface system could have disturbed the currents above the surface, but there was no other way to solve the problem. The thermal images were taken with a Dias Infrared System Proview 380L camera at 120-second intervals.

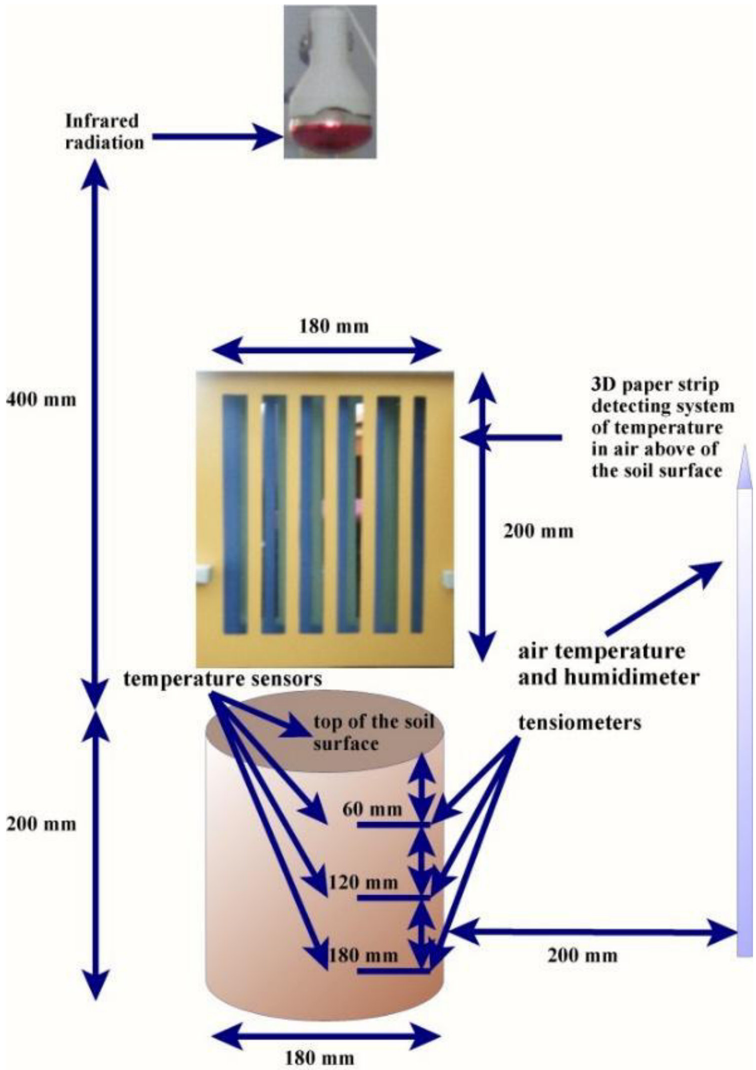

Figure 2: Schematic diagram of the experimental setup

2.4. Computer evaluation program Thermo for the infrared camera

Using a program called Thermo, we set up the lines that coincide with the line elements of the measurement surface system before starting each measurement. The temperature data are obtained from these lines. Before each measurement was started, 16 vertical lines and 1 horizontal line were set on the surface system, and 7 vertical lines were set on the 50 mm wide and 180 mm long free surface of the soil column slate. In accordance with the measurement surface arrangement, we set five measurement lines on the first and third layers, six on the second layer, and one measurement line on the first layer at the bottom, directly above the soil surface, of the same width. The measurement lines set in the Thermo program are shown in Figure 3.

2.5. Presentation of experimental conditions

The measurements were carried out in a styrofoam enclosure (Figure 4b) in order to minimise external disturbances to the drying process and the measurement results. The opening for the infrared lamp was the only one on the insulating cover. The camera, together with the soil column and the surface system, was located in the enclosure, while the data recorder and computer were kept outside for practical reasons. The complete experimental setup is shown in Figure 4. All sensors (temperature sensors, tensiometers, and combined temperature and humidity sensors) are connected to the data logger (Almemo 2980-9). At the end of the measurements, the data logger's results were converted into Excel spreadsheets using a computer program called AMR (ALMEMO Measurement Reader). The infrared camera was connected directly to the computer, and the temperature data from the measurement line was recorded before being converted into Excel spreadsheets using a program called Thermo. The temperature and moisture content measurements were plotted using Origin Pro 8.5 software to characterise the drying of the soil and the processes that occurred during drying.

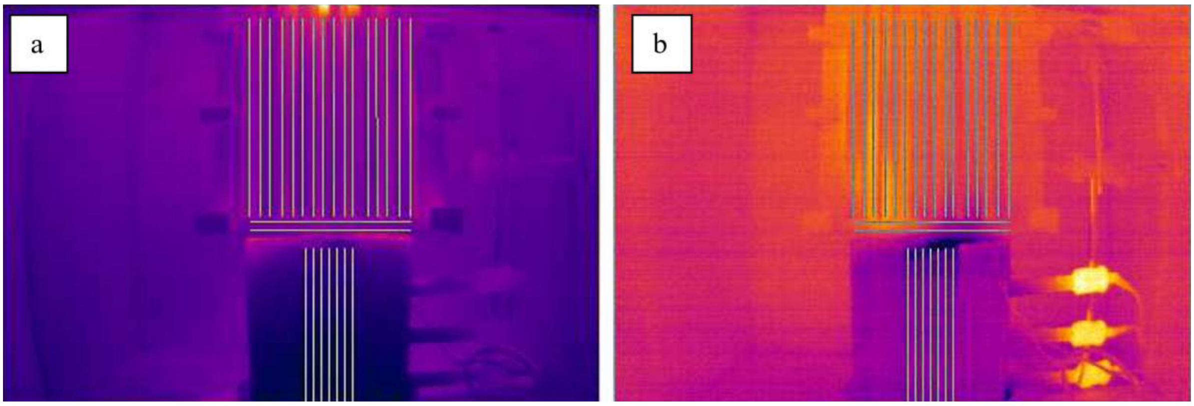

Figure 3: Measurement lines set in the Thermo program (a: illuminated 12-hour period; b: thermal images taken during the unilluminated 12-hour period) for soil column 2.

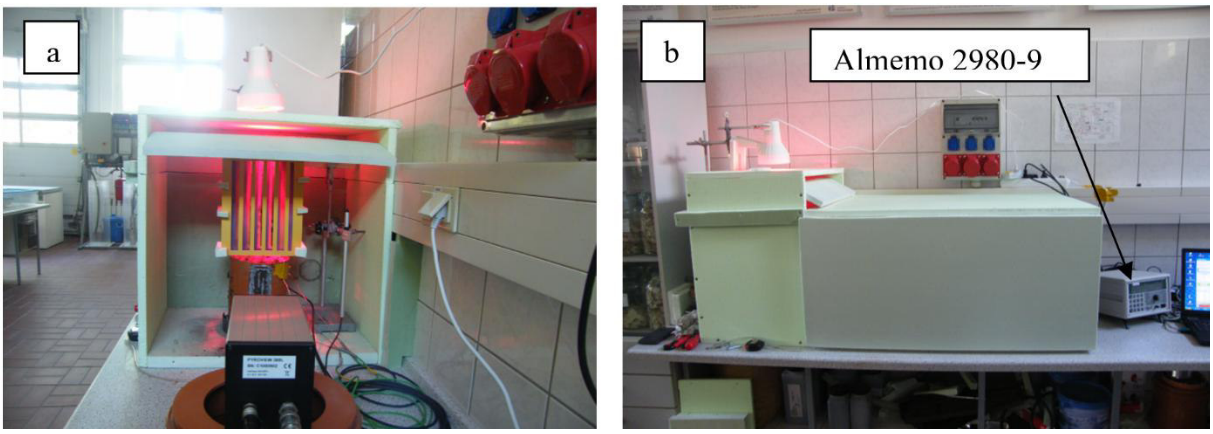

Figure 4: The complete experimental setup (a: without thermal insulation cover, viewed from the thermal camera; b: with thermal insulation cover)

3. RESULTS AND THEIR EVALUATION

When presenting the results, we selected a measurement location from among the strips of paper placed above the soil column and reported it, along with the moisture sensor results.

3.1. Soil column 1, with which we conducted the experiment using the moisture content at the time of sampling

Figure 5 shows the experimental variation in soil moisture conditions and in the moisture content of the air above the soil surface. Changes in soil moisture suction (i.e., tensiometry) are plotted at the three measurement points at depths of 60, 120, and 180 mm from the surface. The current water vapour content, independent of air temperature, provides more accurate information than the relative humidity (f, [%]) about the course of soil water content at the interface, i.e., evaporation through the soil surface, during the experiment. Therefore, the measured values from the combined temperature and relative humidity sensor placed above the soil surface were first converted to vapour pressure using the Magnus-Tettens formula [31] and then to absolute humidity values (a, [g/m^3]) using a simple relationship (0.217*e/T).

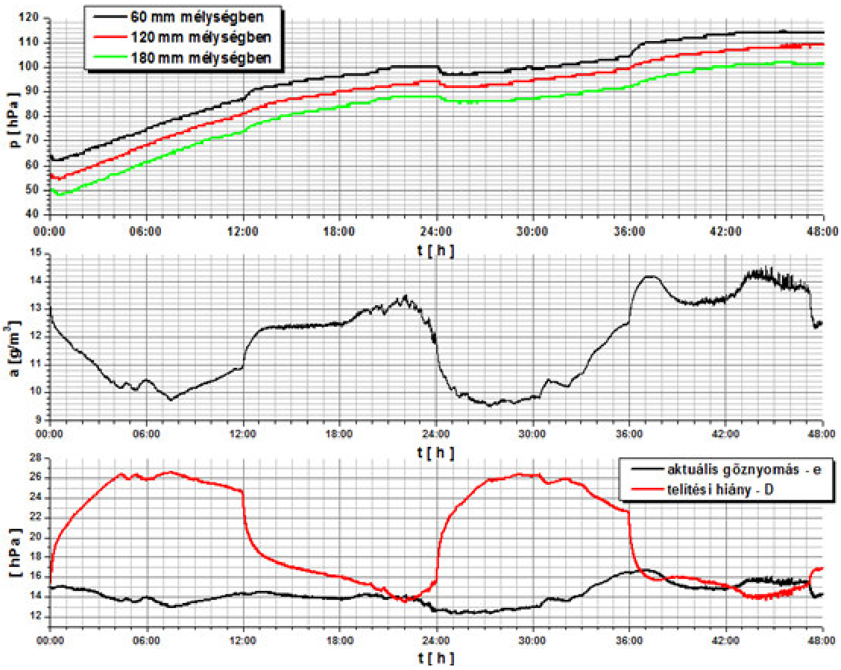

Figure 5: Moisture content changes in the soil and above the soil surface during the experiment conducted with soil column 1

Figure 5 shows that the moisture tensions of the three soil layers are lower at the beginning of the experiment and remain unchanged for about half an hour. Infrared radiation striking the soil surface heats the soil material, and the water content evaporates, so the soil dries continuously during the experiment, increasing the tensiometer reading. From the start of the experiment until 7.5 hours, the moisture content of the air decreases continuously, from an initial level of about 13 g/m^3 to about 9.8 g/m^3, then to 10.8 g/m^3 at 12 hours. Part of the heat gain of the soil material heated by irradiation is used to evaporate the soil's water content at the beginning of the non-illuminated phase. Thus, after 12 hours, the moisture tension values a and, in parallel, the moisture tensor values measured at 3 points in the soil rise steeply, indicating that more evaporation is occurring at the interface, i.e., through the soil surface. The moisture content of the air stabilises at around 12.4 g/m^3 from 13.5 h to 18.5 h, before increasing again to around 13.2 °C by 22.5 h. From 24 hours onward, with the onset of illumination, the air humidity decreases again, reaching around 9.8 g/m^3 by 30.5 hours. The moisture tension increases at 3 measured points on the soil, but with a smaller slope than 12 hours after the start of the experiment. From 30.5 hours onwards, the water vapour content in the air increases steadily, reaching 12.45 g/m^3 at 36 hours. From 36 hours onwards, at the beginning of the non-illuminated period, the a and, in line with this, the moisture tensor values rise steeply again, with increased evaporation through the soil surface, as was the case during the first non-illuminated period. The moisture content of the air rises to 14.2 g/m^3 at 37.5 h, and then to around 13.2 g/m^3 from 32.5 h to 42 h. Thereafter, the air humidity content increases again up to 14.2 g/m^3 and then decreases continuously until the end of the experiment.

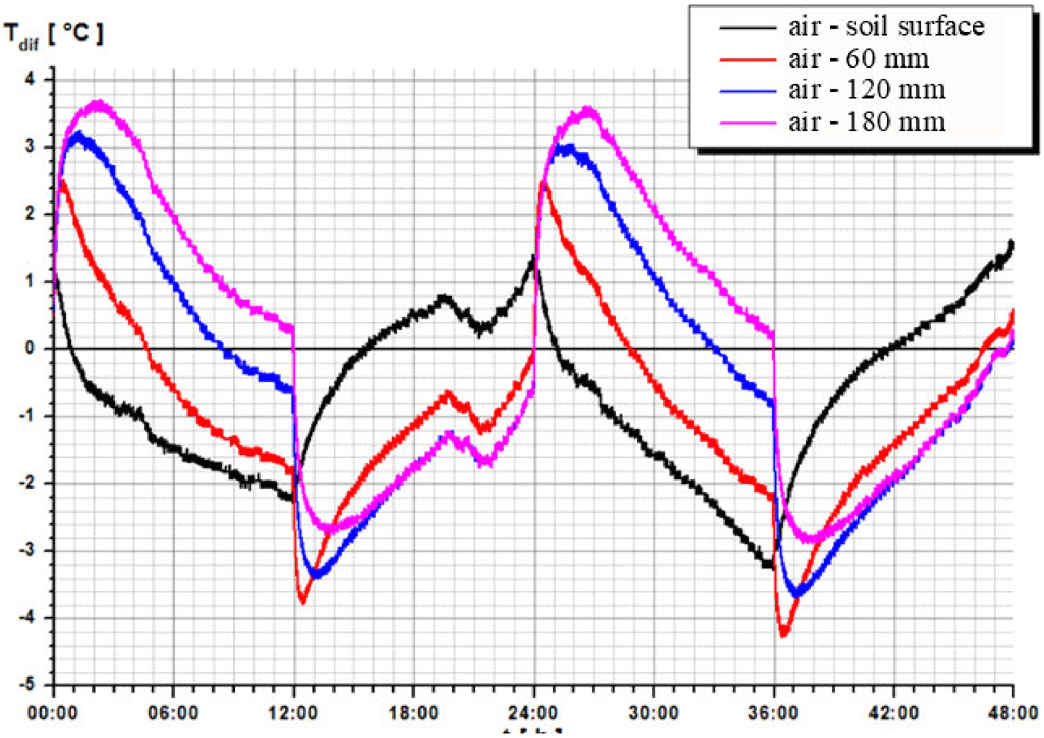

Figure 6: Temperature differences measured between the air and different soil layers

Figure 6 shows the temperature differences between the air and the indicated soil layers. At the start of the experiment, the temperature at all measured soil points was lower than in the air. Infrared rays reaching the soil surface gradually reheat the deeper soil layers due to the soil's thermal conductivity. The soil surface reaches and then exceeds the air temperature after 1 hour, the 60 mm depth after 4.5 hours and the middle level after 8.5 hours. The temperature of the lowest measured point does not reach the air temperature for the first 12 hours. Throughout the period without illumination, the temperatures at the 60 mm, 120 mm, and 180 mm ground points are higher than those in the air. The soil surface cools rapidly, falling below the air temperature after 15.5 hours, as a result of the heat-intensive process of increased evaporation through the soil surface. With the onset of illumination, the air heats up rapidly, the soil follows this process much more slowly, and therefore again the air temperatures are higher than the soil temperatures. Similar trends to those in the first half of the experiment characterise the second half, with the difference that during the last 12 hours of the experiment, without illumination, the temperature at all measured soil points is lower than in the air.

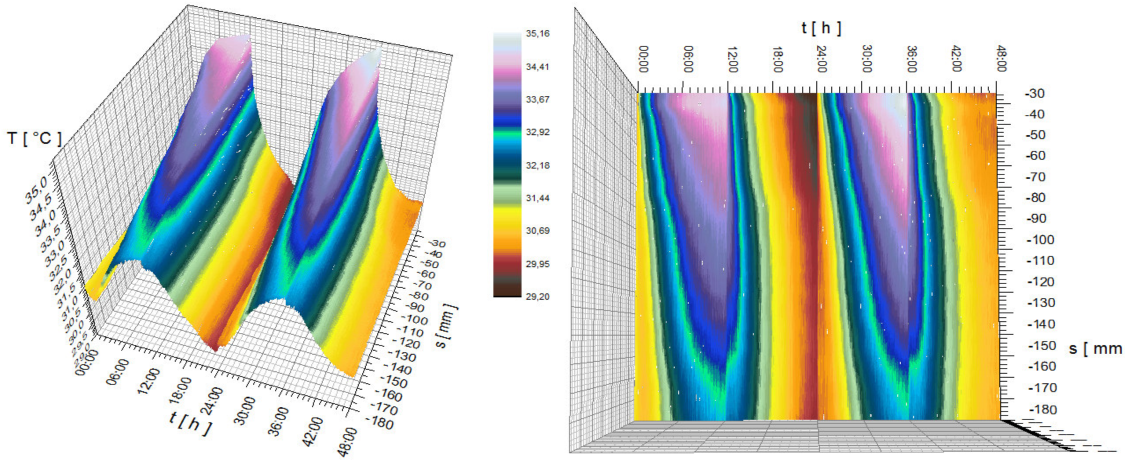

Figure 7: Temperatures measured on the surface of soil column 1 along the vertical measurement line named "Soil L4"

Figure 7 shows the variation in soil temperature, but here plotted continuously with depth from 30 mm to 180 mm below the surface. The measurement line "soil l4", set in the Thermo program for the infrared camera, is drawn vertically on the free soil surface formed on the soil column slate from 30 mm to 180 mm from the surface, with a width of 50 mm. The infrared camera captured thermal images every 2 minutes during the 48-hour experiment. Temperature was plotted as a function of time and distance from the surface. The colour map provides an additional tool for monitoring temperature changes. Overall, temperatures at the surface of the slate are much higher than those within the column along its vertical axis, due to the thin film of air between the soil and the surrounding air in this area, which allows significant heat exchange. At the start of the experiment, temperatures at all measured soil points are nearly identical, around 31 °C. The infrared rays absorbed by the soil surface heat the surface and adjacent layers rapidly, and the soil's thermal conductivity causes the deeper layers' temperatures to rise over time. This change starts at lower levels after 3 to 3.5 hours, with values around 30 °C. By the end of the first 12 hours, distinct temperature ranges with depth have developed. The effect of the vertical heat conduction of the soil is less pronounced on the free surface of the soil column mantle than on the inner soil areas, so that, compared to the sensor measurements, temperature maxima occur shortly after the beginning of the non-illuminated period, followed by a rapid drop in temperature. It can be seen that, well separated from the deeper layers, the soil loses heat more rapidly towards the surface, from a depth of 80 mm, presumably due to increased evaporation in the near-surface layers or convective processes. The deeper areas show a much more uniform pattern of temperature decrease, with slower, more uniform heat loss. The upper 80 mm layer cools to the lowest measured temperatures during the experiment, with uniform values around 29 °C. The lower 140 mm soil layer has a higher temperature of around 30 °C. In the second half of the experiment, similar temperature changes were observed as in the first 24 hours, but with higher values at all points, as already mentioned in the sensor measurement results.

We present here the results for one strip of the data collected by the paper-measuring system above the soil column. In Figure 8, the temperature values of the measurement line "L13" set in the Thermo program are shown as a function of time and distance from the top of the surface element on the third vertical surface element of the first layer of the measurement surface system. The measurement line is 220 mm long; the starting point is the uppermost point of the surface element towards the infrared lamp, and the end point, i.e., point 0, is the ground surface. The temperature of the upper 100 mm of the measurement line is directly influenced by the infrared lamp's radiation, not by the temperature of the surrounding air. It follows that between 0 and -100 mm, both illuminated sections have much higher temperatures. The temperature between -100 and -220 mm is independent of the direct radiation. These problems do not occur during the 12-hour periods without illumination. Part of the infrared radiation is absorbed by the ground surface, but as heat flows into the ground, the ground surface re-radiates about 80% of the long-wavelength infrared back towards the air. The effect of this is clearly visible in the temperature values of the lower 20 mm of the measurement line in both illumination stages, where higher values are observed in the air layers between -200 and -100 mm. At the start of the non-illuminated periods, the temperature drops steeply to about 32°C along the entire length of the measurement line ("L13"). The effect of the intense convective mass and heat flux associated with increased evaporation, especially during these periods, is reflected in the temperature changes, which are clearly visible in the colour map along the entire length of the measured line.

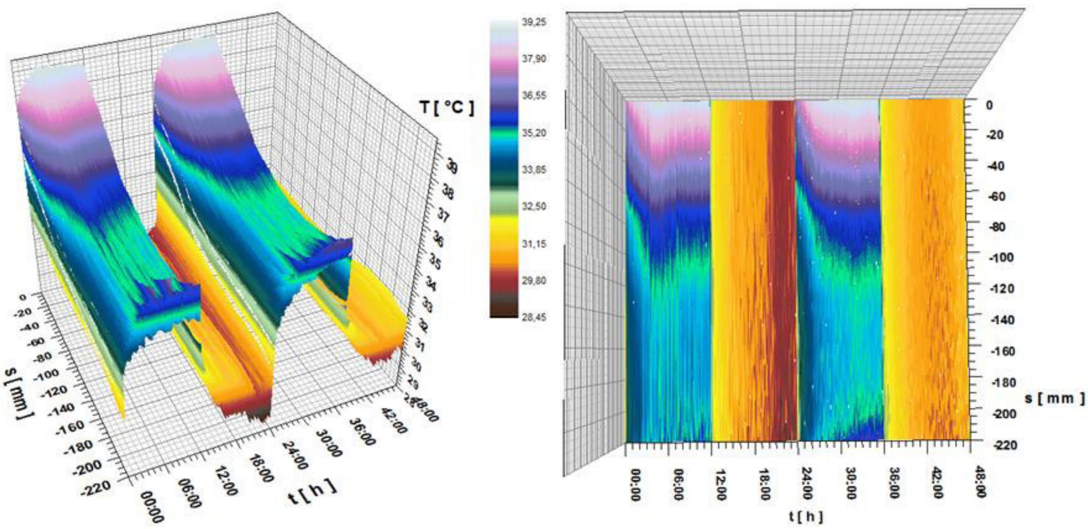

Figure 8: Temperature values of the measurement line named "L13" set on the third vertical surface element of the first layer of the measurement surface system

3.2. Results and evaluation of soil column 2 saturated with water and frozen

Prior to the experiment, the column containing meadow soil was saturated with water through its porous structure using a closed water-distillation system. The saturation process took approximately 24 hours. We exposed the soil sample to 12 hours of freezing before starting the experiment. The markings in Figure 9 are the same as in the previous experiments. It can be seen that at the beginning of the experiment, the temperature at all measured soil points is around the freezing point. At a depth of 60 mm, the temperature is slightly higher than at the soil surface. At the lower two depths, it is slightly lower. While the soil surface warms rapidly and reaches and exceeds the air temperature about 7.5 hours after the start of the experiment, the deeper layers remain frozen, with no increase in temperature. Melting starts after 1 hour 40 minutes at 60 mm from the surface, 120 and 180 mm at about the same time, after 3 hours. At the beginning of the 12-hour non-irradiated phase, the surface and air temperatures fall steeply. Afterwards, the surface temperature remains higher than the air temperature for 3 hours, then falls below it. The high moisture content at this time implies that evaporation is intense, mainly leading to decreases in the near-surface layers and surface temperature. The heat flux into the soil during the experiment decreases with depth, and a phase shift is observed in the deeper layers, due to the soil's thermal conductivity. Thus, the deeper layers reach their maximum temperature after 12 hours without irradiation, i.e., after the cessation of further energy input, after about half an hour at the 60 mm level, 1 hour at the 120 mm level, and 1.5 hours at the 180 mm depth. After 13 hours, the temperatures at depths of 60 mm and 120 mm are approximately the same until the start of the next illumination phase at 24 hours. Compared with the lowest depth of 180 mm, the higher depths heat up less. The temperature characteristics of the next 24 hours are similar to those observed in the same half of the previous experiments. Figure 10 shows variations in moisture content across the different soil layers and in the air above the soil surface. The readings of the tensiometers placed in the soil are given in hPa. It can be seen that at the beginning of the experiment, the moisture absorption in all three soil layers stagnates and then decreases. This means that the liquid water content of the thawing frozen soil remains unchanged until thawing, after which it increases, and the amount of solid water decreases accordingly. The tensiometer can only measure the suction force of the liquid water in the soil, not the solid water. Therefore, after the initial stagnation, the values decrease in parallel with the melting. In all 3 layers, the values begin to increase at about the same time, after 6 hours, as the soil water content begins to evaporate. This process can be clearly followed by the change in absolute humidity(a), which shows a continuous increase. At the beginning of the non-illuminated phase, from 12 h, the humidity of the air increases suddenly with a steep slope, and continues to increase until 20 h, when it reaches 14.5 g/cm^3, compared with the value at the end of the illuminated phase at 12 h, which was around 11.7 g/cm^3. This sudden increase is accompanied by a steep rise in soil moisture content, which decreases due to intense evaporation. From about 20 hours onward, the air humidity begins to decrease, as reflected in the stagnation of the tensiometer readings. From 24 hours onwards, the air humidity drops steeply, and with it the soil moisture tensiometry. After 26 hours, there is a steady increase in the air humidity and a steady decrease in the soil moisture. From 36 hours onwards, similar changes in soil and air moisture content are observed as in the 12 hours to 24 hours interval, but with significantly lower values, as the soil has dried out substantially since the beginning of the experiment and its moisture content has decreased.

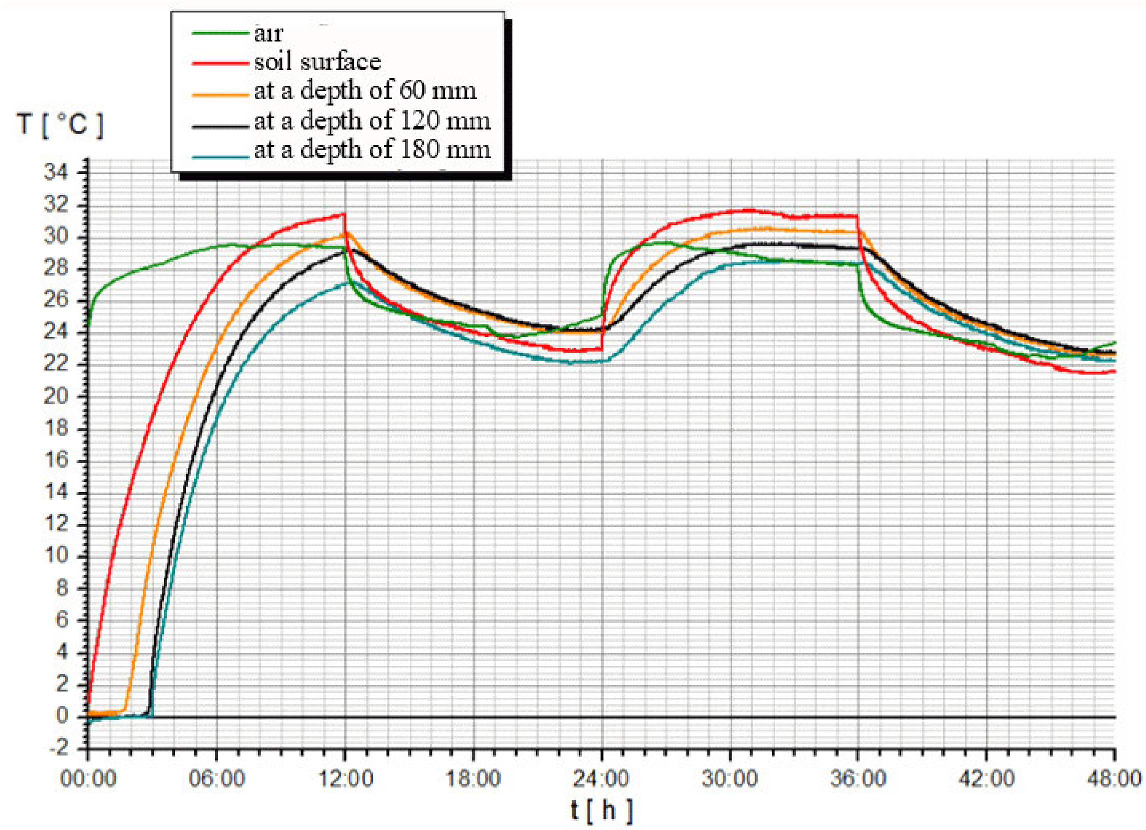

Figure 9: Temperature changes in the soil and above the soil surface during the experiment with soil column 2

Figure 10 shows variations in moisture content across the different soil layers and in the air above the soil surface. The readings from the tensiometers placed in the soil are given in hPa. It can be seen that at the beginning of the experiment, the moisture absorption in all three soil layers stagnates and then decreases. This means that the liquid water content of the thawing frozen soil remains unchanged until thawing, after which it increases, and the amount of solid water decreases accordingly. A tensiometer measures only the suction of water in the liquid phase in soil and does not measure the forces associated with water bound to the solid phase. Therefore, after the initial stagnation, the values decrease in parallel with the melting. In all 3 layers, the values begin to increase at about the same time, after 6 hours, as the soil water content begins to evaporate. This process can be clearly followed by the change in absolute humidity(a), which shows a continuous increase. At the beginning of the non-illuminated phase, from 12 o'clock, the humidity of the air increases suddenly with a steep slope, and continues to increase until 20 o'clock, when it reaches 14.5 g/cm^3, compared with the value at the end of the illuminated phase at 12 o'clock, which was around 11.7 g/cm^3. This sudden increase is accompanied by a steep rise in soil moisture content, which decreases due to intense evaporation. From about 20 h onward, the air humidity begins to decrease, as reflected in the stagnation of the tensiometer readings. From 24 h onwards, the air humidity drops steeply, and with it the soil moisture tension. After 26 hours, there is a steady increase in the air humidity and a steady decrease in the soil moisture. From 36 hours onwards, similar changes in soil and air moisture content are observed as in the 12 h to 24 h interval, but with significantly lower values, as the soil has dried out substantially since the beginning of the experiment and its moisture content has decreased.

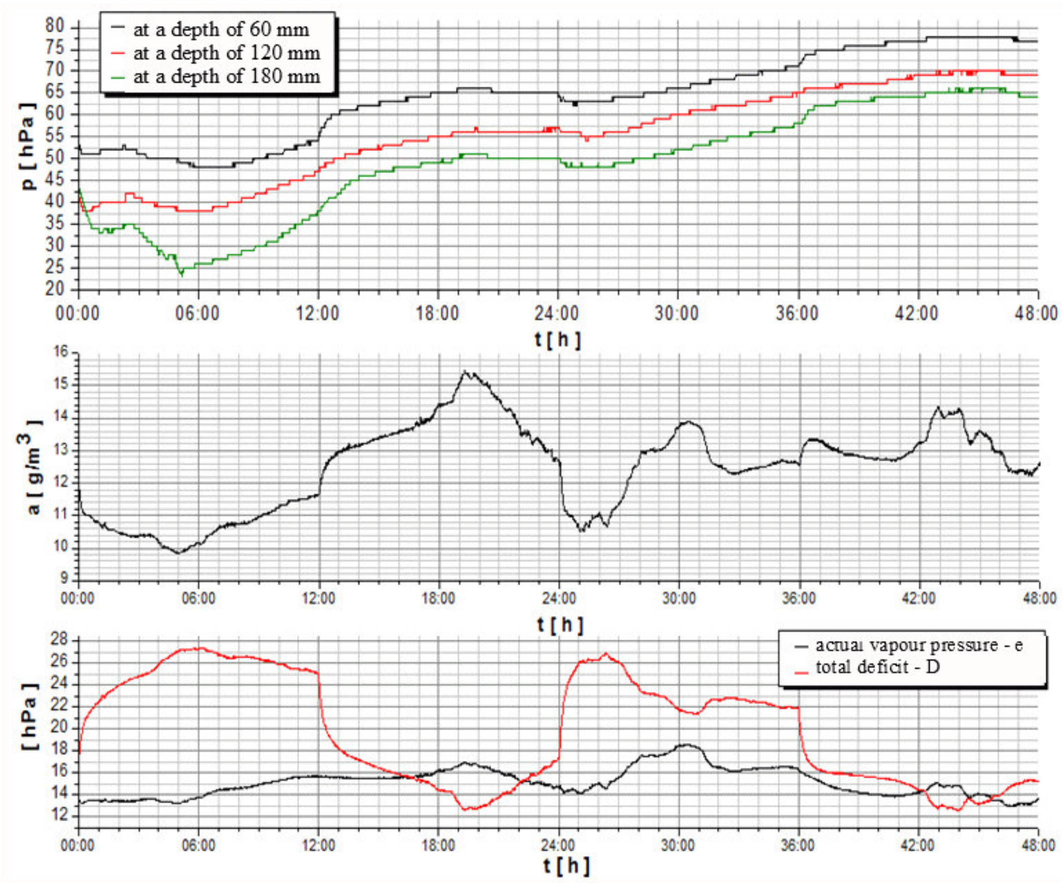

Figure 10: Moisture content changes in the soil and above the soil surface during the experiment with soil column 2

Figure 11 also shows the variation in soil temperature with depth up to 180 mm below the soil surface. The measurement line "soil l4", set in the Thermo program for the infrared camera, is drawn vertically along the free soil surface of the soil column slate to a depth of 180 mm, with a width of 50 mm. The camera took thermal images every 2 minutes during the 48-hour experiment. Temperature was plotted as a function of time and distance from the surface. The colour map further helps to interpret the temperature variation. Understandably, the surface of the slate reaches much higher temperatures than the interior of the column along its vertical axis, due to contact with the surrounding air. The lowest temperatures are around 10°C, compared to the interior of the soil column along the longitudinal axis, where temperatures were near freezing at the start of the experiment and remained so throughout. The heat flux to the shale surface decreases less with depth during the experiment, and heat conduction is lower than in the soil interior, due to continuous energy transfer between the air and the soil. The colour map clearly shows that the layers near the soil surface lose much more heat than the lower layers during the non-illuminated period, partly due to continuous contact between the soil surface and the air and the energy-intensive evaporation of soil water.

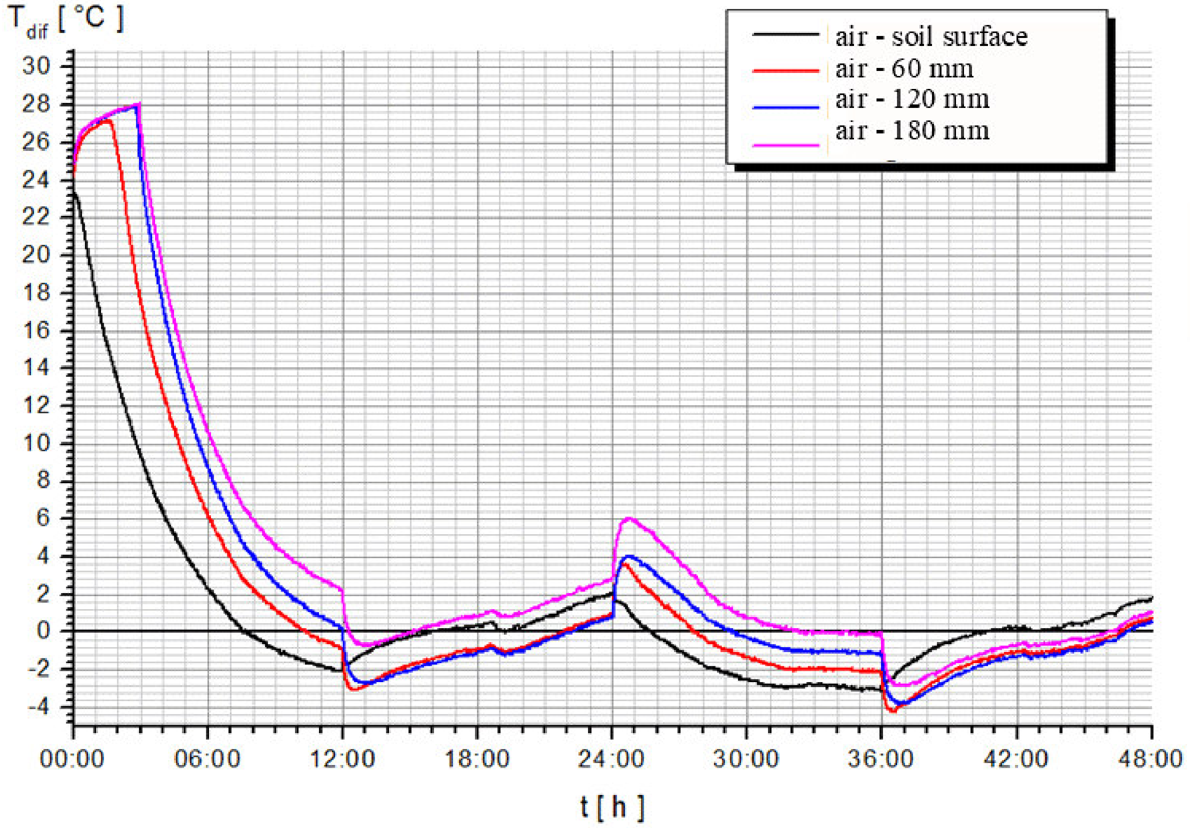

Figure 11: Temperature differences measured between the air and different soil layers

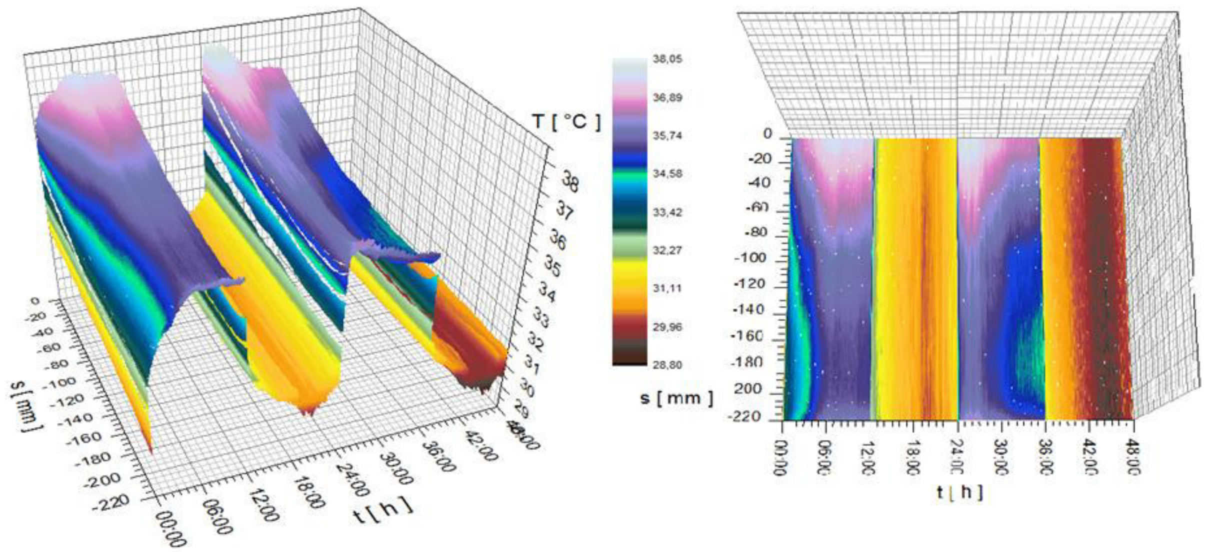

Figure 12: Temperature change on the surface of soil column 2 along the vertical measurement line named "Soil L4"

Figure 12 shows the temperature differences between the air and the other measurement points. It can be seen that the soil surface temperature increases continuously from the beginning of the experiment, faster than the air temperature, and reaches and exceeds the air temperature after 7.5 hours. Initially, the temperature difference between the other measurement points increases compared to the air. The ground is still frozen, but the air temperature is increasing. Here again, as shown in Figure 9, thawing starts after 1.5 hours at a depth of 60 mm and almost simultaneously at the bottom two measuring points after 3 hours. At 60 mm from the surface, the temperature reaches and exceeds the surface air temperature after 10 and a half hours, and at 120 mm just after 12 hours, at the beginning of the 12-hour period without irradiation. The lowest measuring point reaches and exceeds the air temperature only at the beginning of the non-irradiation period, when the air temperature decreases in the absence of irradiation. At a depth of 180 mm, the temperature is higher for 15 hours, and at the ground surface for 15 hours and 50 minutes compared to the surrounding air. The soil surface loses heat due to the heat-absorbing effect of intense evaporation and, presumably, convection, whereas the lowest point of measurement after freezing is not warmed by the 12-hour irradiation like the upper layers and therefore has lower temperatures than the surrounding air. At 60 mm and 120 mm from the surface, the soil continues to cool relative to the air, almost simultaneously, after 22 hours. With the onset of illumination, the temperature differences at all points increase relative to the air, due to the different heat capacities of soil and air. With depth, the temperature difference increases due to thermal conduction, and then the values at different depths decrease over time and exceed the air temperature. The values at the lowest measurement point and the air temperature are approximately the same from 32h to 36 h; the other measurement points continue to warm relative to the air temperature. For the last period without illumination, ground temperatures remain uniformly above air temperatures for 46 hours and fall below air temperatures only in the 2 hours before the end of the experiment.

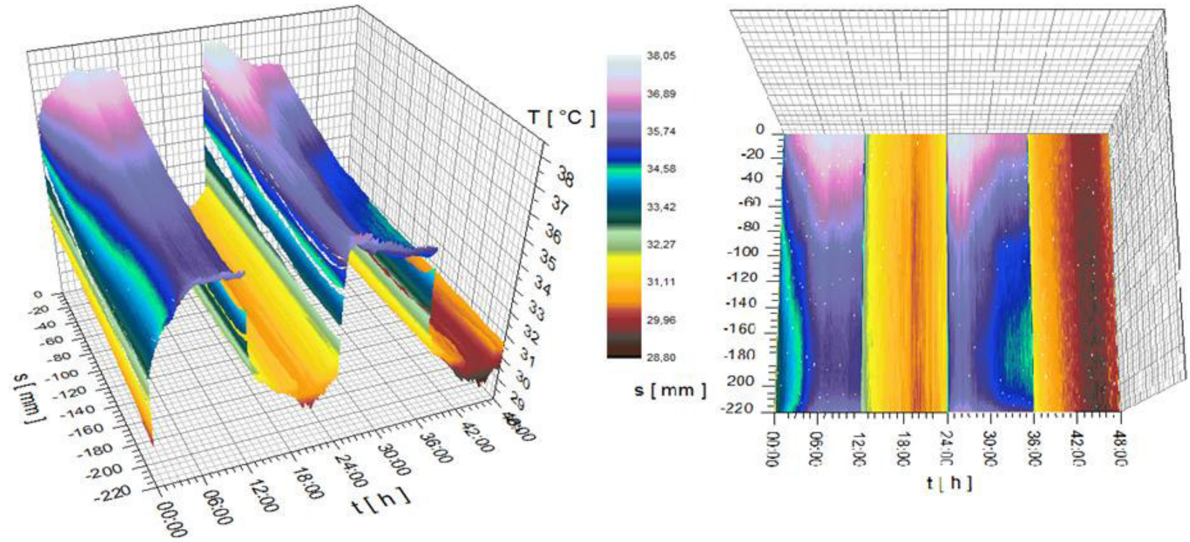

Figure 13: Temperature values of the measurement line named "L23" set on the third vertical surface element of the second layer of the measurement surface system above soil column 2.

In Figure 13, the temperature values of the measurement line "L23" set in the Thermo program are shown as a function of time and distance from the top of the surface element on the third vertical surface element of the second layer of the measurement surface system. The measurement line was 220 mm long; the starting point is the uppermost point of the surface element toward the infrared lamp, and the end point is the point toward the ground surface. It can be seen that the temperature evolution in the air above the ground shows a different pattern from that in previous experiments. The colour map clearly shows that from the beginning of the experiment until about 5 hours after the start, the temperature is significantly lower in the air layer between -130 mm above the top of the measurement line and the last measurement point towards the ground surface. The air layers above -130 mm reach increasingly higher temperatures (as they are directly heated by infrared radiation). The initially frozen ground surface is in constant contact with the air and exposed to continuous infrared radiation, and these two effects combine to accelerate soil thawing. By 3 hours, the entire soil has thawed, as evidenced by the accelerating rate of increase in surface air temperature from this time. The melting of the soil, because it draws heat away from its surroundings, results in significantly lower values in the above-ground air at temperatures below -130 mm. From 5 am to 12 noon, the temperature trend is uniform. From 12 noon, the temperature in the air drops sharply because infrared radiation does not heat the air, and the ground surface is cooler, so the surface radiation is lower. From 24 h onwards, at the start of the second illumination phase, the air warms rapidly to around 35.5 °C in the air layer between -80 mm and -220 mm, then drops from 29 h onwards due to the heat-absorbing effect of increasing evaporation. The moisture content of the air increases markedly at this time, reaching a maximum of 14 g/m^3. Over the last 12 hours without illumination, the temperature trend is similar to that of the first period, but with lower values overall.

4. CONCLUSIONS AND SUGGESTIONS

In this paper, the drying of soil columns under infrared radiation was investigated. Using an infrared lamp to simulate the sun, we measured temperature and moisture changes in the soil and in the air layer above the soil surface using sensor and infrared camera measurements to describe the water and energy balance of the soil, similar to the work of Gao et al. [33]. The instrumentation and setup of the experimental system developed enabled a coordinated measurement process. I have interpreted and described the changes by plotting the sensor and infrared camera measurements. The measurement system designed to monitor flow conditions above the ground surface during the experiment can be considered a result of the experimental work. Despite its many shortcomings, the experiment can provide a good starting point for future work on soil water and energy balance. Some suggestions are therefore made on how and by what methods the efficiency of the experiment could be improved and how a more accurate picture of temperature, moisture and flow conditions could be obtained:

- The use of temperature sensors at several points in the soil could provide a more accurate picture of soil temperature variations.
- More accurate measurements of soil thermal conductivity require the use of a sensor capable of measuring the heat flux into the soil.
- In order to determine the pF curve (The pF curve is a curve describing the water retention capacity of soil, showing the relationship between soil water content and soil water suction (matrix potential)), it is necessary to measure the moisture content of the soil, in addition to measuring the moisture tensiometry values, where possible.
- Measurement of the intensity of infrared radiation reaching the soil surface is recommended.
- Monitoring the variation in soil surface moisture content could be achieved by installing an additional tensiometer.
- Further development of the above-ground measurement surface system is needed to improve accuracy.
- Where possible, thermal images should be taken at a higher frequency, both at the surface of the soil column and in the air layer above the soil surface.
- A plastic tube containing the soil sample should be replaced with a material with better thermal insulation properties.

5. ACKNOWLEDGEMENT

The authors would like to thank the ATB in Potsdam (Germany) for enabling the measurements.

6. REFERENCES

[1] Oke, T. R.: *BOUNDARY LAYER CLIMATES* (2ND ED.), ROUTLEDGE, ISBN-10: 0416044328, ISBN-13: 978-0416044324, LONDON, UK, (1987) https://doi.org/10.4324/9780203407219

[2] Brutsaert, W.: *HYDROLOGY: AN INTRODUCTION*. CAMBRIDGE UNIVERSITY PRESS, ISBN-10: 0521824796, ISBN-13: 978-0521824798, CAMBRIDGE, UK, (2005), http://dx.doi.org/10.1017/cbo9780511808470

[3] Monteith, J. L., Unsworth, M. H.: *PRINCIPLES OF ENVIRONMENTAL PHYSICS: PLANTS, ANIMALS, AND THE ATMOSPHERE* (4TH ED.), ACADEMIC PRESS, OXFORD, UK, (2013) http://dx.doi.org/10.1016/B978-0-12-386910-4.00013-5

[4] Hillel, D.: *ENVIRONMENTAL SOIL PHYSICS*. (1ST ED.), ACADEMIC PRESS, EBOOK ISBN: 9780080544151, SAN DIEGO, CA, USA, (1998)

[5] DE VRIES, D. A.: *THERMAL PROPERTIES OF SOILS*. IN W. R. VAN WIJK (ED.), *PHYSICS OF PLANT ENVIRONMENT,* NORTH-HOLLAND PUBLISHING COMPANY, AMSTERDAM, NETHERLANDS, (1963), PP. 210–235

[6] Jury, W. A., Horton, R.: SOIL PHYSICS (6TH ED.), WILEY, ISBN: 978-0-471-05965-3, HOBOKEN, NJ, USA, (2004)

[7] Wang, R., et al.: SOIL TEMPERATURE EXCEEDING AIR TEMPERATURE AND SURFACE ENERGY FLUX LINKAGES, *ENVIRON. RES. LETT.*, **VOL.** 19, (2024), NO 10, 104029, PP. 1-12, https://doi.org/10.1088/1748-9326/ad7279

[8] Liang, A. et al.: MULTI-SCALE TEMPORAL AND SPATIAL VARIATIONS OF SOIL HEAT FLUX UNDER VARYING RIPARIAN FORESTS: FROM A DAY TO A YEAR. *JOURNAL OF ENVIRONMENTAL MANAGEMENT*, **VOL.** *373*, (2025), 123825, PP. 1-13,

https://doi.org/10.1016/j.jenvman.2024.123825

[9] Alexander, G.: SIMULATING LAND-ATMOSPHERE COUPLING IN THE CENTRAL VALLEY, CALIFORNIA: INVESTIGATING SOIL, **VOL**. 317, (2022), 108898, PP. 1-17,

https://doi.org/10.1016/j.agrformet.2022.108898

[10] Taheri, M. et al.: ENERGY-BASED APPROACHES IN ESTIMATING ACTUAL EVAPOTRANSPIRATION FOCUSING ON LAND SURFACE TEMPERATURE: A REVIEW OF METHODS, CONCEPTS, AND CHALLENGES, *ENERGIES*, **VOL.** 15, (2022), NO 4, 1264, PP. 1-57, https://doi.org/10.3390/en15041264

[11] Zhou, W., et al. GROUND HEAT FLUX RECONSTRUCTION USING BAYESIAN UNCERTAINTY QUANTIFICATION MACHINERY AND SURROGATE MODELING. *EARTH AND SPACE SCIENCE,* **VOL.** 11, (2024), NO 3, e2023EA003435, PP. 1-21, https://doi.org/10.1029/2023EA003435

[12] Benson, D. O., Dirmeyer, P. A.: THE SOIL MOISTURE–SURFACE FLUX RELATIONSHIP AS A FACTOR FOR EXTREME HEAT PREDICTABILITY IN SUBSEASONAL TO SEASONAL FORECASTS. *JOURNAL OF CLIMATE*, **VOL.** 36, (2023), NO 18, PP. 6375-6392, https://doi.org/10.1175/JCLI-D-22-0447.1

[13] Chandrasekhar, S.: *HYDRODYNAMIC AND HYDROMAGNETIC STABILITY*, OXFORD UNIVERSITY PRESS, (1961), OXFORD, UK

[14] Getling, A. V.: *RAYLEIGH–BÉNARD CONVECTION: STRUCTURES AND DYNAMICS*. ADVANCED SERIES IN NONLINEAR DYNAMICS, **VOL**. 11, WORLD SCIENTIFIC, ISBN: 978-981-279-635-6, (1998), SINGAPORE, https://doi.org/10.1142/3097

[15] Stull, R. B.: *AN INTRODUCTION TO BOUNDARY LAYER METEOROLOGY*, KLUWER ACADEMIC PUBLISHERS, ISBN: 978-90-277-2768-8, (1988), DORDRECHT, NETHERLANDS, https://doi.org/10.1007/978-94-009-3027-8

[16] Garratt, J. R.: *THE ATMOSPHERIC BOUNDARY LAYER*, CAMBRIDGE UNIVERSITY PRESS, (1992), CAMBRIDGE, UK

[17] Zhang, L. N., et al. LAND SURFACE INFLUENCE ON CONVECTIVE AVAILABLE POTENTIAL ENERGY AND WEATHER SYSTEMS. *JOURNAL OF HYDROMETEOROLOGY*, **VOL.** 24, (2023), NO 8, PP. 1561–1578, https://doi.org/10.1175/jhm-d-22-0191.1

[18] Gao, Y., et al.: INFLUENCE OF SOIL MOISTURE VARIABILITY ON ATMOSPHERIC BOUNDARY LAYER DEVELOPMENT, *JOURNAL OF CLIMATE*, **VOL**. 36, (2023), NO 12, PP. 5689–5709. https://doi.org/10.1175/jcli-d-22-0446.1

[19] Yang, D., et al.: DISTRIBUTED SOIL MOISTURE IMPACTS ON SURFACE ENERGY PARTITIONING AND CONVECTIVE INITIATION, *JOURNAL OF GEOPHYSICAL RESEARCH: ATMOSPHERES,* **VOL.** 126, (2021), NO 12, e2020JD033893. https://doi.org/10.1007/s00704-022-04046-z

[20] Liu, W., et al.: THE INFLUENCE OF SOIL MOISTURE ON CONVECTIVE ACTIVITY: A REVIEW, *THEORETICAL AND APPLIED CLIMATOLOGY*, **VOL**. 149, (2022), NO 1, PP. 221-232, https://doi.org/10.1007/s00704-022-04046-z

[21] Philip, J. R., de Vries, D. A.: MOISTURE MOVEMENT IN POROUS MATERIALS UNDER TEMPERATURE GRADIENTS, *TRANSACTIONS, AMERICAN GEOPHYSICAL UNION*, **VOL**. 38, (1957), NO 2, PP. 222–232, https://doi.org/10.1029/TR038i002p00222

[22] Lu, N., Likos, W. J.: *UNSATURATED SOIL MECHANICS*, WILEY, ISBN-10: 0471447315, ISBN-13: 978-0471447313, (2004), HOBOKEN, NJ, USA https://doi.org/10.1038/s43017-023-00448-7

[23] Gaona, J., et al.: INTERACTIONS BETWEEN PRECIPITATION, EVAPOTRANSPIRATION AND SOIL MOISTURE-BASED INDICES TO CHARACTERIZE DROUGHT WITH HIGH-RESOLUTION REMOTE SENSING AND LAND-SURFACE MODEL DATA, *NATURAL HAZARDS AND EARTH SYSTEM SCIENCES DISCUSSIONS*, **VOL**. 22, (2022), NO 10, PP. 1-30, https://doi.org/10.5194/nhess-22-3461-2022

[24] Bhattacharya, B. K., et al.: A COUPLED GROUND HEAT FLUX–SURFACE ENERGY BALANCE MODEL OF EVAPORATION USING THERMAL REMOTE SENSING OBSERVATIONS. *BIOGEOSCIENCES*, **VOL**. 19, (2022), NO 23, PP. 5521-5551, https://doi.org/10.5194/bg-19-5521-2022

[25] Lazić, I., et al.: IMPACT OF SOIL TEXTURE IN COUPLED REGIONAL CLIMATE MODEL ON LAND-ATMOSPHERE INTERACTIONS, *THEOR APPL CLIMATOL,* **VOL**. 156, (2025), NO 165, PP. 1-23, https://doi.org/10.1007/s00704-025-05393-3

[26] KUMAR, D., ET AL.: REMOTE SENSING OF SOIL MOISTURE DYNAMICS: APPLICATIONS IN AGRICULTURE, HYDROLOGY AND CLIMATE STUDIES, *INTERNATIONAL JOURNAL OF PLANT & SOIL SCIENCE*, **VOL.** 37, (2025), NO 8, PP.730-750, https://doi.org/10.9734/ijpss/2025/v37i85673

[27] Monteith, J. L., Unsworth, M. H.: *PRINCIPLES OF ENVIRONMENTAL PHYSICS: PLANTS, ANIMALS, AND THE ATMOSPHERE* (4TH ED.), ACADEMIC PRESS, ISBN-10: 0123869102, ISBN-13: 978-0123869104, (2013), OXFORD, UK, https://doi.org/10.1016/B978-0-12-386910-4.00013-5

[28] Yin, D., et al.: SPATIOTEMPORAL ANALYSIS OF SOIL MOISTURE VARIABILITY AND ITS DRIVING FACTOR, *REMOTE SENSING*, **VOL.** 15 (2023), NO 24, 5768, PP-1-18, https://doi.org/10.3390/rs15245768

[29] Chen, F., Dudhia, J.: COUPLING AN ADVANCED LAND SURFACE–HYDROLOGY MODEL WITH THE PENN STATE–NCAR MM5 MODELING SYSTEM. PART I: MODEL IMPLEMENTATION AND SENSITIVITY, *MONTHLY WEATHER REVIEW*, **VOL.** 129, (2001), NO 4, PP. 569-585, https://doi.org/10.1175/1520-0493(2001)129<0569:caalsh>2.0.co;2

[30] Ek, M. B. et al.: IMPLEMENTATION OF NOAH LAND SURFACE MODEL ADVANCES IN THE NATIONAL CENTERS FOR ENVIRONMENTAL PREDICTION OPERATIONAL MESOSCALE ETA MODEL, *JOURNAL OF GEOPHYSICAL RESEARCH: ATMOSPHERES*, **VOL.** 108, (2003), NO D22, PP. GCP 12-1-16, https://doi.org/10.1029/2002JD003296

[31] Lawrence, M. G.: THE RELATIONSHIP BETWEEN RELATIVE HUMIDITY AND THE DEWPOINT TEMPERATURE IN MOIST AIR: A SIMPLE CONVERSION AND APPLICATIONS, *BULLETIN OF THE AMERICAN METEOROLOGICAL SOCIETY,* **VOL**. 86, (2005), NO 2, PP. 225–233, https://doi.org/10.1175/BAMS-86-2-225

[32] Várallyay, Gy.: *A MEZŐGAZDASÁGI VÍZGAZDÁLKODÁS TALAJTANI ALAPJAI,* AKADÉMIAI KIADÓ, ISBN-10: 963-9256-82-4, ISBN-13: 978-963-9256-82-8, (2002), BUDAPEST, MAGYARORSZÁG

[33] Gaoa, Z. et al.: DETERMINATION OF SOIL TEMPERATURE IN AN ARID REGION, *JOURNAL OF ARID ENVIRONMENTS*, **VOL.** 71, (2007) PP. 157–168. https://doi.org/10.1016/j.jaridenv.2007.03.012

Corresponding address:
Dr. habil. Agnes BÁLINT
Department/Laboratory: Institute of Environmental Engineering and Natural Sciences
Faculty: Sándor Rejtő Faculty of Light Industry and Environmental Engineering
University/Company: Óbuda University
Address of Institution/Company: Doberdó str. 6.
Postal code, City, State: 1034 Budapest, Hungary
E-mail: balint.agnes@uni-obuda.hu